PHYSICAL REVIEW A VOLUME 17, NUMBER 3 MARCH 1978

Electronic relativistic and Coulomb deflection effects on $1s\sigma$-vacancy production

R. Anholt*
Department of Physics, Stanford University, Stanford, California 93405
(Received 18 July 1977)

Measurements of K-vacancy production cross sections are reported for 0.5- to 3.5-MeV/amu H, He, O, F, and Cl bombardments of selected elements between Y and U. Ratios of H- to He-induced cross sections corrected for binding effects are compared with proposed Coulomb-deflection correction factors. The validity of the Kocbach factor is confirmed. Ratios of experimental H- and He-induced cross sections to plane-wave Born-approximation cross sections, corrected for binding and Coulomb-deflection effects, agree with theoretical relativistic correction factors calculated in the preceding paper. A new semiempirical formula for predicting $1s\sigma$-vacancy production cross sections is derived. The overall agreement of the new formula with H-, He-, O-, F-, Cl-, Kr-, and Xe-induced cross sections is generally within experimental uncertainties (10%–20%).

I. INTRODUCTION

To predict K-vacancy production cross sections in the higher-Z (Z_H) collision partner in encounters with projectiles with small charges, the plane-wave Born approximation (PWBA)[1-3] or semiclassical approximation (SCA)[4-8] has been used. In the PWBA, the cross section is proportional to the square of the matrix element of the Coulomb potential between the projectile nucleus and the atomic electron, taken between initial and final states of the projectile and target electron.[1] Usually, nonrelativistic one-electron atomic $1s$ and continuum wave functions are used to describe the initial and final electronic states. Plane waves are used to describe the projectile's motion. Three corrections must be made to the PWBA to predict $1s\sigma$-vacancy production cross sections. First, a Coulomb-deflection correction[9,10] must be made because the projectile, instead of passing by the target nucleus (Z_2) along a straight-line trajectory, will be deflected by the Coulomb field of the target nucleus. This deflection inhibits K-vacancy production. Second, an electronic relativistic correction must be made since nonrelativistic $1s$ and continuum wave functions become increasingly inappropriate as Z_H increases.[3,6,7] Finally, a correction should be made for the change in the effective binding energy of the target electron that is induced by the presence of the projectile charge.[9,10] Another way of stating this is to say that in sufficiently slow collisions, excitation occurs from a molecular orbital (MO) instead of an atomic orbital (AO).[11] To produce K vacancies in the higher-Z collision partner in very asymmetric collisions, the electron must be excited out of the lowest ($1s\sigma$) MO.[9,12]

Vacancy production in the $1s\sigma$ MO has been discussed by Anholt and Meyerhof (Ref. 10, henceforth referred to as paper III). However, to better understand the electronic relativistic and Coulomb-deflection effects, measurements of many K-vacancy production cross sections in high-Z target atoms induced by 0.5- to 3-MeV/amu H, He, O, F, and Cl ions were made. Previously only a few high-Z, low-velocity cross sections had been measured.

A new semiempirical formula to predict $1s\sigma$-vacancy production is derived in this paper. Essentially, we modify the formulas that predict K-vacancy production by low-Z projectiles such as protons. We find that the $1s\sigma$-vacancy production cross section can be written as a product of the PWBA cross section, a Coulomb-deflection correction factor C, an electronic relativistic correction factor R, and a binding correction factor B.

The new semiempirical relations differ from those derived in paper III in three ways. First, it is found in Sec. IV that the Brandt Coulomb-deflection correction factor,[9,10] used previously, does not correctly predict the Coulomb-deflection effect for low-Z_1 projectiles (protons and alpha particles) and hence presumably also high-Z projectiles. Kocbach recently made exact SCA calculations of the Coulomb-deflection correction factor using Rutherford trajectories.[8] His deflection factor, which is considerably smaller than the Brandt factor, correctly predicts ratios of proton-induced to effective-deuteron-induced K-vacancy production cross sections in high-Z target atoms. Therefore the Kocbach Coulomb-deflection correction factor is incorporated into the new semiempirical formulas. Second, since few cross sections for heavy-ion-induced K-vacancy production in high-Z elements were available previously, the proposed relativistic correction could not be tested adequately. Also PWBA calculations of atomic relativistic correction factors R showed that the Bang-Hansteen equation[4,6] used in the pre-

vious formula underestimates the relativistic correction factor for large values of the minimum momentum tranfer needed to ionize the K electron. Therefore the PWBA relativistic correction factor is incorporated into the new semiempirical formulas. Third, in paper III, the semiempirical cross sections were normalized to the proton-induced K-vacancy cross sections measured for the same Z_2 and ion velocity v_1.[10] This normalization was necessary because the formula failed to accurately predict the proton-excitation cross section. With the new Coulomb-deflection and relativistic correction factors, however, experimental proton cross sections can be predicted to an accuracy of ±10%. Therefore normalization to experimental proton cross sections is unnecessary.

Section II of this paper describes our measurements, and Sec. III discusses theories of the binding, Coulomb-deflection, and electronic relativistic effects. To derive semiempirical relations (Sec. IV), we begin by examining H- and He-induced cross sections. In these bombardments the binding and other $1s\sigma$-MO effects are small, so that direct comparison between theoretical calculations of the Coulomb-deflection and relativistic correction factors and experiment is possible. After establishing the relativistic and Coulomb deflection factors for protons (atomic correction factors), we then use our heavy-ion excitation data to fit the binding correction factor and other parameters needed to describe the $1s\sigma$-MO influence on the relativistic and Coulomb-deflection correction factors. Finally the experimental cross sections are compared with the complete semiempirical expression.

II. EXPERIMENT

The Stanford 3-MV Van de Graaff was used to obtain 0.4- to 2.4-MeV proton beams. The Stanford FN tandem Van de Graaff was used to obtain 0.5- to 3.5-MeV/amu He, O, F, and Cl ion beams. The beam was directed onto a thick target tilted 45° from the beam toward the x-ray detector. An intrinsic-Ge detector with a pulsed optoamplifier and pileup-rejector system viewed the target at right angles to the beam through a 0.25-mm mylar window. A 1.6-mm Al absorber was used to attenuate unwanted L x-ray radiation. The detector efficiency was determined by placing calibrated radioactive sources directly at the beam spot.

The entire target chamber acted as a Faraday cup. A 300-V electron suppressor was used between the collimator and chamber. We verified that the x-ray yield is independent of electron suppressor voltage for voltages greater than 300 V. (Using no suppressor, approximately 20% lower yields were obtained.) Detector deadtime was measured by using the beam integrator to trigger a number of pulses into the detector preamplifier. The total number of pulser counts surviving in the x-ray spectrum was compared with the number of triggers to give the counting system deadtime.[12]

Thick-target K x-ray yields, Y_x, were obtained in the usual way.[12] Yields were measured at 4–7 different bombarding energies E_1, and the resulting $\log Y_x$ values were least-square fitted to polynomials in the $\log E_1$. This allowed interpolation of values of Y_x and dY_x/dE_1 at convenient values of E_1. The Merzbacher-Lewis formula was used to convert yields to cross sections. Electronic stopping powers were obtained using the He-ion tabulation of Ward *et al.*[14] and Forster's formulas for effective projectile charges.[15] Straggling and recoil effects[16] are negligible in these measurements. Charge exchange effects[17] may be present in the Cl + Y, . . . , Sn data. For this reason, these data were not used in the fitting procedure described below. We have previously shown that charge exchange effects are negligible in O, F + Z_2 > 37 K-vacancy production data.[10] The resulting K-vacancy cross sections, obtained by dividing K x-ray cross sections by single-vacancy fluorescent yields,[18] are listed in Table I.

The thick-target yield method is certainly not the most accurate method for obtaining K-vacancy cross sections.[19] We attempted to measure cross sections as small as 1 μb in this work. Therefore the use of thick targets instead of thin targets was necessary. Uncertainties in the x-ray yields consisted of the following components: beam integration, ±10%; detector efficiency, ±10%; detector deadtime, ±5%; counting statistics, <5%; and fluorescent yields, <5% ($\omega_K > 0.7$ always). An additional uncertainty in measurements of atomic Sm, Ho, Hf, Ta, Re, and Pt K vacancies (and to a lesser extent Au, Th, and U K vacancies) is generated in subtracting the contribution of the K-shell internal conversion decay of Coulomb excited nuclear states from the observed K-vacancy yield. To obtain the yield of K vacancies made by γ-ray internal conversion, γ-ray yields were measured at 90° with respect to the beam and were multiplied by theoretical internal-conversion coefficients.[20] Besides the relative uncertainties in measuring x-ray and γ-ray yields (detector efficiency and counting statistics), there are two other uncertainties in the yield of internal-conversion K vacancies. First, we assume that the γ-rays are emitted isotropically. Anisotropies as large as 20% may be present.[21] Second, the internal-conversion coefficient for mixed $M1/E2$ γ-ray transitions depends on the $M1/E2$ mixing coefficient which is generally

TABLE I. K-vacancy production cross sections. Typical errors ±25% (see text).

Proton-induced

E_1 (MeV)	Y (b)	Mo (b)	Ag (b)	Sn (mb)	Pr (mb)	Sm (mb)	Ho (mb)	Hf (mb)
0.5	0.051	0.018	0.0034	1.2	0.042	...	...	...
0.75	0.26	0.098	0.022	9.3	0.68	0.46	0.12	0.053
1	0.77	0.30	0.076	34	3.6	2.3	0.75	0.39
1.25	1.7	0.68	0.18	85	10	6.8	2.6	1.4
1.5	3.1	1.3	0.36	170	21	15	6.4	3.1
2	7.3	3.2	0.95	470	70	46	20	9.7
2.5	13	5.9	2.0	890	160	96	44	22

E_1 (MeV)	Ta (mb)	Re (mb)	Pt (mb)	Au (mb)	Pb (mb)	Bi (mb)	U (mb)
0.75	0.035	0.023	0.012	0.008	0.0027	0.0019	...
1	0.032	0.17	0.13	0.097	0.063	0.056	...
1.25	1.7	0.77	0.53	0.40	0.25	0.25	0.037
1.5	2.9	2.2	1.3	1.0	0.68	0.62	0.13
2	9.1	7.4	4.2	3.3	2.4	2.0	0.60
2.5	21	10	9.6	7.8	5.3	5.1	2.1

Alpha-particle–induced

E_1 (MeV/amu)	Y (b)	Mo (b)	Ag (b)	Sn (mb)	Pr (mb)	Sm (mb)	Ho (mb)	Hf (mb)
0.75	1.1	0.43	0.12	56	6.1	4.6	1.9	1.2
1	2.9	1.2	0.33	170	23	16	9.1	4.5
1.25	5.9	2.4	0.71	370	52	37	21	11
1.5	10	4.4	1.3	680	100	69	37	20
2	23	10	3.1	1700	250	170	82	49
2.5	44	20	6.2	3300	540	340	180	100
3	74	30	10	5300	880	550	290	170

E_1 (MeV/amu)	Ta (mb)	Re (mb)	Pt (mb)	Au (mb)	Pb (mb)	Bi (mb)	Th (mb)	U (mb)
0.75	0.70	...	0.27	...	...	...	...	...
1	3.4	3.1	1.4	1.4	0.91	0.78	0.33	0.23
1.25	8.9	7.4	4.1	3.6	2.4	2.2	0.91	0.71
1.5	17	14	9.0	7.6	5.0	4.7	2.1	1.8
2	42	35	26	20	14	14	6.9	6.1
2.5	86	68	49	42	31	29	16	12
3	150	110	85	70	52	48	26	23

Oxygen-induced

E_1 (MeV/amu)	Y (b)	Mo (b)	Ag (b)	Sn (b)	Sm (b)	Ho (b)
0.75	3.2	1.6	0.53	0.28	0.033	0.014
1.0	9.2	4.5	1.7	0.87	0.12	0.063
1.25	21	10	3.4	2	0.31	0.14
1.5	41	21	8	3.9	0.71	0.34
2.0	120	57	21	11	1.8	1
2.5	270	120	44	23	3.7	2
3.0	540	230	70	44	6.4	3.2
3.5	990	370	120	73	9.9	5.0

TABLE I. (*continued*)

Oxygen-induced (continued)

E_1 (MeV/amu)	Ta (mb)	Pt (mb)	Au (mb)	Pb (mb)	Bi (mb)	U (mb)
0.75	6.4	2.9	2.9	1.5	1.4	···
1.0	31	14	13	7.6	7.6	···
1.25	93	39	37	24	20	7.3
1.5	160	87	83	56	45	19
2.0	510	270	240	180	140	65
2.5	900	560	510	370	320	150
3.0	1600	890	850	630	590	280
3.5	2300	1200	1200	890	960	440

Fluorine-induced

E_1 (MeV/amu)	Y (b)	Mo (b)	Ag (b)	Sn (b)	Sm (b)	Ho (b)	Ta (b)
0.75	3.0	1.5	0.47	0.26	0.042	···	0.008
1.0	8.8	4.4	1.4	0.8	0.13	0.063	0.031
1.25	20	10	3.3	1.9	0.28	0.13	0.070
1.5	41	20	6.5	3.7	0.56	0.35	0.173
2.0	120	52	18	10	1.5	0.89	0.470

E_1 (MeV/amu)	Pt (mb)	Au (mb)	Pb (mb)	Bi (mb)	Th (mb)	U (mb)
0.75	4.3	2.8	2.3	2.9	1.7	···
1.0	18	13	11	12	6.0	5.8
1.25	49	38	31	33	15	13
1.5	100	83	68	72	33	27
2.0	280	250	200	210	100	93

Chlorine-induced

E_1 (MeV/amu)	Y (b)	Mo (b)	Ag (b)	Sn (b)	Sm (b)	Ho (b)	Ta (b)
0.667	1.1	0.48	0.17	0.10	···	0.0054	0.0023
0.75	1.9	0.82	0.28	0.19	···	0.013	0.0061
1.0	7.0	2.8	0.94	0.59	0.12	0.062	0.031
1.25	19	7.3	2.3	1.4	0.3	0.17	0.086
1.5	43	17	4.9	3.0	0.74	0.41	0.22
2.0	150	59	16	8.3	1.8	1.2	0.64

E_1 (MeV/amu)	Pt (mb)	Au (mb)	Pb (mb)	Bi (mb)	Th (mb)	U (mb)
0.667	···	1.1	···	···	···	···
0.75	···	3.1	···	···	···	···
1.0	···	16	···	···	···	···
1.25	55	50	36	35	17	11
1.5	130	120	86	85	53	34
2.0	460	380	270	280	210	140

not well known.[20] The measured Re, Ho, and Pt $1s\sigma$ cross sections are least accurate because of uncertainties in the $M1/E2$ coefficient. The atomic K x-ray yield is defined as the difference between the measured yield and the yield of internal-conversion K x rays.

Excluding nuclear internal conversion, the major experimental uncertainty is in the determination of dY_x/dE_1. Although polynomial fits of the $\log Y_x$ to the $\log E_1$ can be used to reproduce $Y_x(E_1)$ accurate

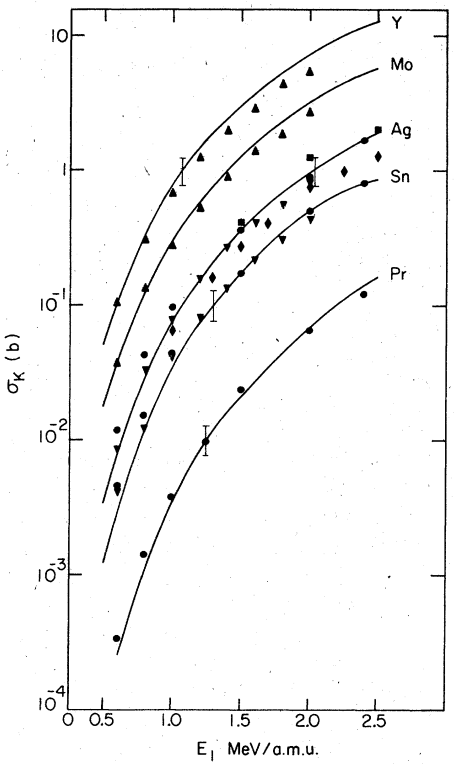

FIG. 1. K-vacancy production cross sections by protons. Our thick-target results (line) are compared with other thin-target measurements (points). Symbols: ●: Ag, Pr, Sn (Ref. 29); ▲: Y, Mo (Ref. 19); ▼: Ag, Sn (Ref. 26); ■: Ag (Ref. 25); ♦: Ag (Ref. 22). Typical cross-section uncertainties are ±25% in the thick-target measurements, and ±10% in thin-target measurements monitored by Rutherford scattering (Ref. 19).

to 5%, the derivatives differed by as much as 20% when polynomials of different degrees were used. We used polynomials of degree 3, 4, and 5, and carefully compared each fit to select proper values of dY_x/dE_1 where different fits gave different results. The uncertainty in the stopping powers used to convert yields to cross section is less than 5%.[25]

Figure 1 compares proton-induced Y, Mo, Ag, Sn, and Pr K-vacancy cross sections measured by the thick-target-yield method to the thin-target results of other experimenters.[19,22-35] The agreement is clearly very good and gives us confidence that our cross sections are accurate to ±25% (excluding internal conversion effects). Our measured O-, F-, and Cl-induced cross sections are also compared with thin-target measurements in Figs. 10–12. Agreement within ±25% between our thick-target measurements and other thin-target measurements[30,36-38] is obtained for the heavy-ion bombardments also.

III. THEORY

The PWBA and SCA theories of K-vacancy formation are discussed in Refs. 1–8. In the nonrelativistic PWBA, the cross section may be obtained from[2]

$$\sigma_{\mathrm{PWBA}} = 8\pi a_0^2 Z_1^2/Z_2^4 F(\eta_K,\theta_K)/\eta_K , \tag{1}$$

where $Z_1(Z_2)$ is the atomic number of the lighter (heavier) collision partner, $Z_2^* = Z_2 - 0.3$, $I_K = Z_2^{*2}\mathfrak{R}$, $\theta_K = U_K/I_K$,

$$\eta_K = (v_1/v_K)^2 = E_1/(A_1 I_K \lambda), \tag{2}$$

a_0 is the Bohr radius, U_K is the K-binding energy of the heavier partner, and λ is the ratio of the proton mass to the electon mass. A similar relation can be obtained using the SCA.[5] Tables of the dimensionless F function calculated with the PWBA and SCA are available.[2,5] The PWBA and SCA F functions are numerically identical to within 20% for $v_1/v_K < 0.5$. In our work, we used the PWBA exclusively[12] because $F_{\mathrm{SCA}}(\eta_K,\theta_K)$ is not tabulated for sufficiently low values of η_K. (When we began this work, we were not aware of the addendum to Ref. 5 published by Kocbach.[8])

The PWBA does not predict $1s\sigma$-vacancy production cross sections accurately in the systems of interest to us. To obtain $1s\sigma$-vacancy production cross sections, the PWBA cross section is multiplied by binding (B), Coulomb-deflection (C), and relativistic (R) correction factors, described in the following sections:

$$\sigma_{1s\sigma} = \sigma_{\mathrm{PWBA}} BCR . \tag{3}$$

A. Binding

In collisions with positively charged projectiles, the target electrons will be partly attracted to the projectile. If the collision is slow enough (as in the present cases, where $v_1/v_K < 1$), the most tightly bound target electrons may form MO's around the projectile and target nuclei.

In very asymmetric collisions K vacancies observed in the heavier collision partner are made in the $1s\sigma$ MO.[10-13] As the projectile atomic charge Z_1 is increased, the binding energy of the $1s\sigma$ electron at the internuclear distance of closest approach ($R = 0$) increases approximately as $(Z_1+Z_2)^2$, so that it becomes more difficult to excite the $1s\sigma$ electron. Cross sections measured at constant ion velocities increase more slowly than Z_1^2 as predicted by Eq. (1). Around $Z_1 \simeq 15$, the cross section (depending on Z_2 and v_1) reaches a maximum and actually decreases with larger projectile charge.[10]

Various theoretical or semiempirical relations have been proposed to account for this effect.[9,10]

Anholt and Meyerhof[10] proposed a semiempirical binding correction factor B given by

$$B=\left(\frac{U_K}{U_{\mathrm{UA}}}\right)^{n(\xi_K)}, \tag{4}$$

where $n(\xi_K)$ is an empirically derived function of the inverse of the reduced mimimum momentum transfer $q_0 a_K$:

$$\xi_K=(q_0 a_K)^{-1}=(4\eta_K)^{1/2}. \tag{5}$$

U_K is the K-binding energy of the higher-Z collision partner, and U_{UA} is the K-binding energy in the united (Z_1+Z_2) atom. The function $n(\xi_K)$ is derived in Sec. IV D of this paper.

B. Coulomb deflection

The PWBA and usually the SCA theories implicitly assume that the projectile traverses the atom without being deflected in the target's nuclear electric field.[1,2,5] Since the major contribution to the K-vacancy cross section comes from impact parameters b of the order of $r_{ad}\sim q_0^{-1}=\hbar v_1/U_K$ (typically 10^{-11} cm) (Ref. 4) and the ion is deflected significantly only in trajectories with $b\sim d=Z_1Z_2e^2/E$ (typically 10^{-12} cm; E is the center-of-mass energy), this approximation is generally good. However, with decreasing ion velocities (smaller r_{ad} and larger d values), the use of the straight-line-trajectory approximation becomes less accurate.

Bang and Hansteen[4] developed a SCA for K-vacancy production which used Rutherford trajectories. They showed that the Coulomb-deflection correction factor C can be obtained approximately from

$$C=e^{-\pi d q_f}, \tag{6}$$

where $q_f=(U_K+E_f)/\hbar v_1$ and E_f is the electron continuum energy. Brandt *et al.*[9] integrated this factor over continuum states E_f and obtained

$$C_{\mathrm{B}}=9E_{10}(\pi d q_0)\simeq\frac{9}{9+\pi d q_0}e^{-\pi d q_0}, \tag{7}$$

where E_{10} is the exponential integral of order 10.[9]

The Bang-Hansteen-Brandt Coulomb-deflection factor is only an approximation. Recently Kocbach[8] calculated proton+Au K-vacancy production cross sections exactly using nonrelativistic electron wave functions and Rutherford trajectories. His results for the Coulomb-deflection factor can be written approximately as

$$C_K=(0.22+0.78e^{1.9\pi d q_0})^{-1}. \tag{8}$$

The function C_K decreases much more rapidly with increasing $\pi d q_0$ than C_B. Kocbach points out that the cross section obtained with Rutherford trajectories is given by an infinite series with terms alternating in sign. Hence using only the first term in the series to obtain C_B gives a correction factor which is too large.

C. Relativistic effects

Most PWBA and SCA theories make use of nonrelativistic electronic 1s and continuum wave functions.[1,2,5] The essential difference in the Dirac electronic configuration wave functions is that close to the nucleus, they behave as $r^{\gamma-1}$, where $\gamma=(1-\alpha^2Z_2^2)^{1/2}$ and $\alpha=137^{-1}$. This weak divergence at $r=0$ transforms to an increased density of high-momentum components in the electronic momentum wave function. Therefore momentum transfer from the projectile to the target K electron is more efficient with relativistic wave functions, and larger cross sections are expected and observed.

One can define a relativistic correction factor by the ratio of the K-vacancy production cross section calculated using relativistic wave functions to the nonrelativistic cross section. Amundsen *et al.*[6] made a theoretical investigation of relativistic correction factors calculated using the SCA and Anholt[13] calculated relativistic correction factors using the PWBA.[3] Several approximate correction factors are also available.[6] A simple empirical formula was derived[13] to accurately fit the PWBA correction factors. Defining $Q=q_0a_K(\equiv\xi_K^{-1})$. The relativistic correction factor is given by

$$R=\max(R_{\mathrm{BH}},R_{\mathrm{A}}), \tag{9}$$

where

$$R_{\mathrm{BH}}=Q^{4(1-\gamma)}\left[1+(1-\gamma)\frac{\pi}{2}\frac{3+2\gamma}{5+4\gamma}Q\right]^2, \tag{10}$$

$$R_{\mathrm{A}}=G(Z_F)Q^{4(1-\gamma_R)}[1+S(\gamma_R)(Q-Q^{-1}) -(1-\gamma_R)(1-\tfrac{7}{3}Q^{-2})]^2, \tag{11}$$

$$S(\gamma)=\begin{cases}\frac{1}{2}\sin\gamma, & \gamma\geq 0.5\\ \frac{1}{2}, & \gamma<0.5,\end{cases}$$

$\gamma=(1-\alpha^2Z_F^2)^{1/2}$, $\gamma_R=(1-\alpha^2Z_R^2)^{1/2}$, and $G(Z_F)$ and Z_R are empirically determined functions of Z_F.[13] Normally, $Z_F\equiv Z_2$, except as noted below.

D. 1$s\sigma$-MO corrections to the relativistic and Coulomb factors

The relativistic and Coulomb-deflection correction factors quoted in Secs. IV B and IV C are correct only for projectiles with very small nuclear charge, i.e., collisions where the increased binding of the 1$s\sigma$ electron beyond the 1s binding energy is negligible. However, since both factors depend critically on the minimum momentum transfer q_0 (or $Q=q_0a_K$), which in turn depends on the minimum energy transfer U_K, U_{UA}, or some characteristic 1$s\sigma$ binding energy $E_{1s\sigma}$ ($U_K<E_{1s\sigma}$

$< U_{UA}$), it is clear that we cannot apply these atomic correction factors to predict K-vacancy production by high-Z projectiles without further modifications. Lacking *ab initio* calculations of Coulomb-deflection and relativistic correction factors for $1s\sigma$-vacancy production, the modifications to these factors have to be made empirically.

For the Coulomb factor, we followed the suggestion made by Brandt *et al.*,[9] modifying $\pi d q_0$ according to

$$\pi d q_0 \rightarrow \pi d q_0 \epsilon \,, \tag{12}$$

where ϵ is a binding correction parameter. Anholt and Meyerhof[10] required ϵ to approach U_{UA}/U_K in the limit $\xi_K \rightarrow 0$ [$n(\xi_K = 0) \sim 9$; in this limit the adiabatic distance defined by Bang and Hansteen[4] is close to zero, so that all of the excitation occurs at very close internuclear distances where the $E_{1s\sigma} \equiv U_{UA}$.] We used[10]

$$\epsilon = 1 + k \frac{U_{UA} - U_K}{U_K} \frac{n(\xi_K)}{9} \,, \tag{13}$$

with $k = 1$. This equation is retained in the present work. However, as shown below, the value of k must be modified.

We also observed that the relativistic correction factor for 1.4- and 2.4-MeV/amu H, He, O, Cl, Br, and Xe bombardments of Pb increased with the projectile charge. To account for this increase, the definition of Z_F and Q in Eqs. (10) and (11) were modified as follows

$$Q \rightarrow Q_{UA} = U_{UA} a_K / \hbar v_1 \,, \tag{14}$$

$$Z_F \rightarrow Z_2 (1 + \beta Z_1) \,, \tag{15}$$

where β is obtained by fitting the data as described in paper III and Sec. IV D of this paper.

IV. RESULTS

A. Excitation by protons

Proton excitation data can best test the atomic Coulomb-deflection and relativistic correction factors. To begin our discussion of these data, we present in Fig. 2 ratios of 1-MeV proton-induced K-vacancy production cross sections to the PWBA cross section. The data shown includes our own, as well as data taken by many other groups.[19,27-35] The ratios are compared with Coulomb-deflection and relativistic correction factors. Since binding or $1s\sigma$-MO effects cannot be completely neglected, we also show the binding correction factor. Also we have used the binding modifications to R and C given by Eqs. (12)–(15), using the following values of $n(\xi_K)$, β, and k previously obtained in paper III:

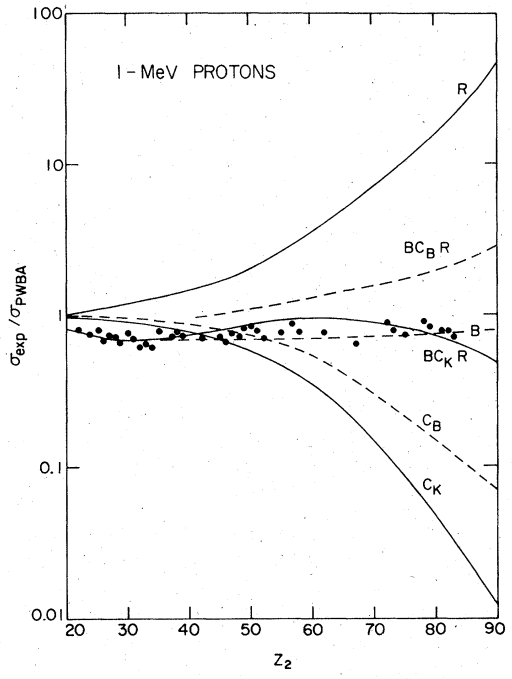

FIG. 2. The ratio of the experimental K-vacancy production cross section for 1-MeV protons to the PWBA prediction (points) compared with various correction factors defined in Eqs. (4)–(5) and (7)–(16).

$$n(\xi_K) = 9.09 - 9.71\xi_K + 6.42\xi_K^2 - 7.45\xi_K^3 \,, \tag{16}$$
$$\beta = 0.0075 \,, \quad k = 1 \,.$$

Since $U_K \approx U_{UA}$, the binding correction factor is nearly unity, 0.7 to 0.8 between Ti and U. The binding modification to R and C changes those values by less than 5%. Hence within this uncertainty, the relativistic and Coulomb-deflection factors shown in Fig. 2 and discussed in Secs. IV B and IV C can be called atomic correction factors. The product $C_K R$ is nearly unity; therefore $BC_K R$ is approximately equal to B. This overall correction factor nearly reproduces the experimental cross section ratio. However, if the Brandt Coulomb-deflection factor is used, the value of $BC_B R$ is between 1 and 2, while most of the data lies between 0.6 and 0.9. This should be an adequate justification for using the Kocbach factor C_K instead of the Brandt factor C_B. However, if for some reason the relativistic effect is overestimated by Eqs. (9)–(11), the Brandt Coulomb-deflection factor may still be correct. (It is unlikely that the binding factor for protons is inaccurate by more than 5%.) Thus, to verify the Coulomb-deflection and relativistic correction factors, the deflection factor should be verified first. This can be done by examining ratios of proton cross sections to alpha cross sections. Once the

Coulomb-deflection (and binding) factors are determined, we can examine the relativistic correction factor.

B. Atomic Coulomb-deflection factors

Since the PWBA cross section and the binding and relativistic correction factors are independent of the mass of the projectile, the ratio of the proton- to deuteron-induced K-vacancy production cross sections for the same ion velocity and target should be[9]

$$\frac{\sigma_p(v_1, Z_2)}{\sigma_D(v_1, Z_2)} = \frac{C(\pi d q_0 \epsilon)}{C(\frac{1}{2}\pi d q_0 \epsilon)} , \tag{17}$$

where C is either C_K or C_B, and here the distance of closest approach d is evaluated for protons.

Equation (17) provides an excellent way of testing the atomic Coulomb-deflection correction factor. However, we found it difficult to make K-vacancy production cross-section measurements using a deuteron beam, because the beam is accompanied by a large flux of neutrons which destroy our solid-state x-ray detectors. Instead we used alpha particles which have the same charge-to-mass ratio as deuterons. Under the same conditions,

$$\frac{4\sigma_p}{\sigma_\alpha} = \frac{C(\pi d q_0 \epsilon_p)}{C(\frac{1}{2}\pi d q_0 \epsilon_\alpha)} \frac{B_p R_p}{B_\alpha R_\alpha} , \tag{18}$$

where B and R are the binding and relativistic correction factors for protons (subscript p) and alpha particles (subscript α). We can still obtain the ratio of the Coulomb-deflection factors by multiplying σ_p/σ_α by the relativistic and binding factors:

$$\frac{\sigma_p}{\sigma_{\text{“}D\text{”}}} = \frac{C(\pi d q_0 \epsilon_p)}{C(\frac{1}{2}\pi d q_0 \epsilon_\alpha)} = \frac{4\sigma_p}{\sigma_\alpha} \frac{B_\alpha R_\alpha}{B_p R_p} . \tag{19}$$

Unfortunately, this method for obtaining the ratio is not model independent since we must assume an equation for the binding and relativistic factors. (Ultimately, we wish to derive the relativistic correction from the data once the Coulomb-deflection correction is understood.) The corrections to $4\sigma_p/\sigma_\alpha$ are not drastic, however. The value of R_α/R_p is of the order of 1.01 – 1.05, and results from the minor modifications to Q and Z_F in Eqs. (14)–(15). Note that typical experimental uncertainties are of the order of 25%. We used the binding correction from Eqs. (4) and (16). The net correction to the ratio $4\sigma_p/\sigma_\alpha$ varies from 0.73 to 0.89 as Table II shows. Hence, we have confidence that $\sigma_p/\sigma_{\text{“}D\text{”}}$ cannot be systematically incorrect by more than 3%–5%, even if reasonably different expressions for the binding and relativistic correction factors are eventually discovered.

The second problem with using $4\sigma_p/\sigma_\alpha$ ratios is that the value of ϵ is different for protons and alpha particles [see Eq. (13)]. It is desirable to plot $\sigma_p/\sigma_{\text{“}D\text{”}}$ vs $\pi d q_0 \epsilon_p$ for many elements and many ion velocities. Unfortunately, different theoretical curves would be obtained for different values of Z_2 and v_1, since ϵ_α and ϵ_p depend on v_1 and Z_2 as Table II shows. As a compromise, in Fig. 3 we plotted $\sigma_p/\sigma_{\text{“}D\text{”}}$ vs $\pi d q_0 \epsilon_a$, where ϵ_a is the arithmetic average of ϵ_p and ϵ_α. Since ϵ_p and ϵ_α differ by only 2%–4%, this is a minor uncertainty.

Figure 3 shows that the Kocbach Coulomb-deflection factor [Eq. (8)] is indeed preferable to the Brandt deflection factor [Eq. (7)]. The experimental uncertainties shown on this curve arise from three sources: uncertainty in the charge integration, in the detector deadtimes, and, most importantly, in the determination of dY_x/dE_1. The placement of the detector in relationship to the beam spot was calibrated very carefully after the proton and alpha experiments; hence the relative geometry coefficient is accurate to 4%. The uncertainty due to the γ-ray internal conversion contribution to the observed K-vacancy yield is not included in the error bars shown in Fig. 13. Although there is a considerable spread in the data, it is pleasing to see that the points are grouped slightly more tightly than the error bars. We conclude that the Kochbach factor accurately predicts the Coulomb-deflection correction factor. Therefore this correc-

TABLE II. Correction factors to $4\sigma_p/\sigma_\alpha$ in Eq. (19).

Z_2	E_1 (MeV/amu)	B_p	B_α	R_p	R_α	F[a]	ϵ_p	ϵ_α
Y	0.75	0.710	0.508	1.495	1.525	0.7304	1.039	1.079
	3	0.842	0.711	1.155	1.173	0.859	1.019	1.040
Pr	0.75	0.764	0.586	3.800	3.940	0.795	1.030	1.062
	3	0.813	0.662	2.025	2.099	0.844	1.023	1.047
U	0.75	0.810	0.657	83.79	89.15	0.862	1.023	1.048
	3	0.831	0.691	17.43	18.58	0.886	1.02	1.042

[a] $F = R_\alpha B_\alpha / B_p R_p$.

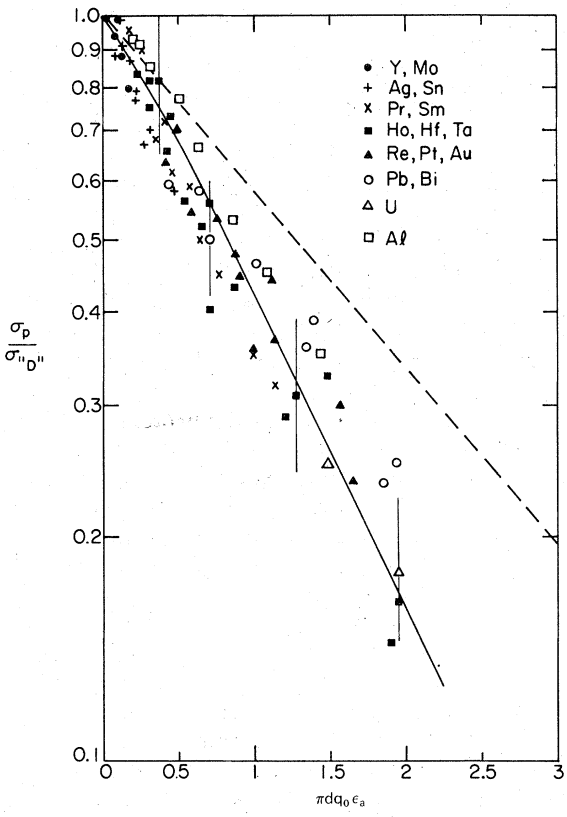

FIG. 3. Ratio of the proton-induced K-vacancy cross section to the effective "deuteron"-induced cross section measured at the same ion velocity vs $\pi dq_0 \epsilon_a$ (defined in text). The ratio is calculated from σ_p/σ_α ratios using Eq. (19). Dashed line: C_B [Eq. (7)]; solid line: C_K [Eq. (8)]. Aluminium points were measured using deuteron and proton beams by Brandt *et al.*, as quoted in Ref. 35.

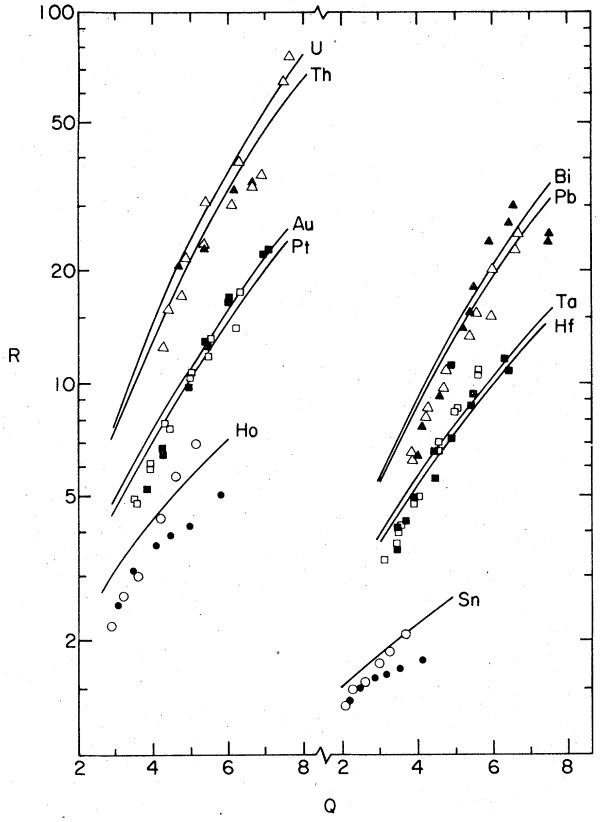

FIG. 4. The relativistic correction factor determined by Eq. (20) vs $Q = U_{UA} a_K/\hbar v_1$. Closed points: proton measurements; open points: alpha measurements. Theoretical correction factors, calculated using Eqs. (9)–(11) and (14)–(16), are shown by the solid lines.

tion factor will be used throughout the remainder of this paper.

C. Atomic relativistic correction factors

With the Coulomb-deflection factor semiempirically determined, and the binding effect small, the relativistic correction factor can be isolated by dividing experimental cross sections by the binding and Coulomb-deflection-corrected PWBA cross sections. We define an experimental relativistic correction factor by

$$R_{\text{exp}} = \sigma_{\text{exp}}/\sigma_{\text{PWBA}} BC_K , \tag{20}$$

where B is given by Eqs. (4) and (16).

In Fig. 4, R_{exp} values for proton and alpha-particle excitation are plotted versus Q as defined in Eq. (14). To simplify this figure, we have not attempted to distinguish between experimental correction factors for adjacent Z_2 values. The data agrees well with the relativistic correction factor based on Eqs. (9)–(11). Although the experimental points are slightly higher than theory for $Q > 4$ and lower for $Q < 4$, the experimental uncertainty of ±25% is larger than the average deviation of these points from theory. Hence we can conclude that within the expected experimental uncertainties, Fig. 4 confirms the validity of Eqs. (9)–(11) for the "atomic" relativistic correction factor ($Z_1 = 1, 2$).

D. $1s\sigma$ excitation

In Secs. IV A–IV C the validity of the atomic relativistic and Coulomb-deflection correction factors was confirmed. Thus Eqs. (1)–(5) and (8)–(15) are guaranteed to accurately predict K-vacancy production cross sections in the limit where $Z_1 \to 0$. To predict K-vacancy cross sections for $Z_1 > 0$, where we have no accurate perturbed-stationary-states calculations as a guide, the binding correction factor and the $1s\sigma$-MO modifications to R and C must be empirically determined. In this section we derive values of $n(\xi_K)$ specifying B [Eq. (4)], k specifying ϵ [Eq. (13)], and β specifying Z_F [Eq. (15)].

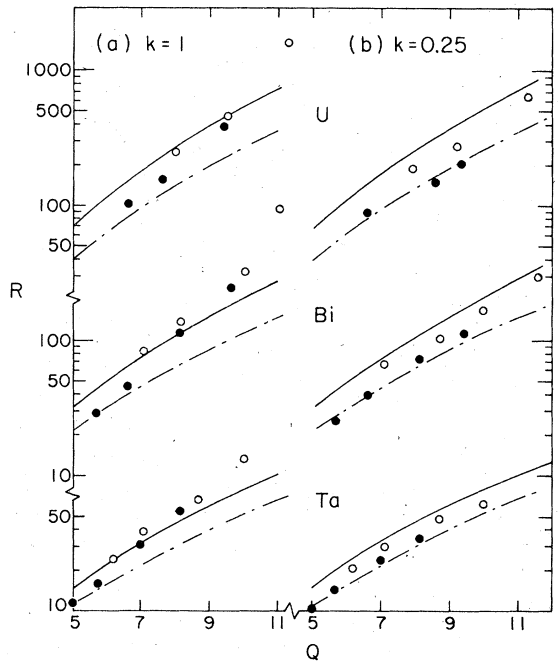

FIG. 5. Relativistic correction factors R_{exp} for Ta, Bi, and U plotted against Q. The R_{exp} values were calculated using Eqs. (20), (4), (5), (8), (12), and (13) with (a) $k=1$ and (b) $k=0.25$. Open points: Cl measurements; Closed points: F measurements. Theoretical curves were calculated using Eqs. (9)–(11), (14), and (15) with $\beta=0.01$ for $Z_L=9$ (dash-dot) and $Z_L=17$ (solid).

The value of k was adjusted so that the experimental relativistic correction factors agree with Eqs. (9)–(11), (14), and (15). In Fig. 5, R_{exp} values [calculated from Eq. (20)] for F- and Cl-induced Ta, Bi, and U K-vacancy production cross sections are plotted against $Q=Q_{UA}$ [Eq. (14)]. The n values from paper III [Eq. (16)] were used to calculate B [Eq. (4)]. In Fig. 5(a) R_{exp} was calculated using $k=1$ to determine the binding correction parameter ϵ [Eq. (13)] used to calculate the Coulomb-deflection correction factor C. In Fig. 5(b), $k=0.25$ was used. The curves in Fig. 5 were obtained for F- and Cl-induced Ta, Bi, and U K-vacancy production using Eqs. (9)–(11), (14), and (15) for the relativistic factor and $\beta=0.01$. We adjusted the value of k so that the R_{exp} values are parallel to the theoretical curves. When $k=1$ was used, the high-Q R_{exp} values increased too steeply with Q, but with the optimum value of $k=0.25$, the R_{exp} values are parallel to the theoretical curves. No attempt was made to make the R_{exp} values agree with the theoretical curves in Fig. 5, or with R values calculated with any given value of β. The k value was adjusted only to give the same slope to R_{exp} as R.

With the value of k fixed, the β and n values can be fitted following approximately the same procedure as in paper III:

(i) Least-squares fit measured H-, He-, Li-, C-, N-, and O-induced K-vacancy production cross sections σ_{exp} in elements with $Z_2<50$ to

$$\log\left(\frac{\sigma_{exp}(Z_1,Z_2,v_1)}{Z_1^2}\right)=-n\log U_{UA}+\text{constant}, \quad (21)$$

keeping Z_2 and v_1 constant. Then least-squares fit the n values for different values of Z_2 and v_1 to a cubic polynomial in ξ_K. Equation (21) can be derived from Eq. (3) assuming that the Coulomb-deflection and relativistic correction factors are nearly unity or that the product of the two factors is independent of Z_1.

(ii) Calculate "experimental" relativistic correction factors for H-, He-, O-, F-, Cl-, Kr-, and Xe-induced K-vacancy production in the heavy elements using Eq. (20). The binding and Coulomb-deflection factors are calculated using Eq. (4) and the n values fitted in step i (or step iii). By comparing R_{exp} values with Eqs. (9)–(11), (14), and (15), a β value for each value of Z_1, Z_2, and v_1 can be obtained. Average the β values.

(iii) Since the relativistic and Coulomb-deflection factors for the low-Z_2 data are not negligible, refit the low-Z_2 cross sections to

$$\log\left(\frac{\sigma_{exp}(Z_1,Z_2,v_1)}{Z_1^2RC}\right)=-n\log U_{UA}+\text{constant}, \quad (22)$$

where R is calculated using Eqs. (9)–(11), (14), and (15) and the averaged β value from step ii, and C is calculated using Eqs. (8), (12), and (13) and the previous n values. Fit the new n values to a polynomial in ξ_K.

(iv) Return to step ii, and repeat steps ii and iii until the low-Z_2 data is self-consistent with the high-Z_2 data. Only three iterations were required to obtain n and β values consistent to within ±1%.

While making the new iterations, the dependence of β on Z_1 was further investigated. In step ii, a β value is obtained for every value of R_{exp}, i.e., every combination of Z_1, Z_2, and v_1 for which a measured cross section is available. After the first iteration, instead of averaging the β values altogether, we averaged the β values for different projectiles (Z_1) separately. In Fig. 6, the final averaged β values for H-, He-, O-, F-, Cl-, Kr(Br)-, and Xe-induced K-vacancy production are plotted against Z_1. The error bars represent the standard deviation in the simple average. The H and He β values have a larger uncertainty than the Kr and Xe values because the Kr and Xe cross sections depend more sensitively on the value of β than H and He cross sections. Generally the scatter in the β value results from

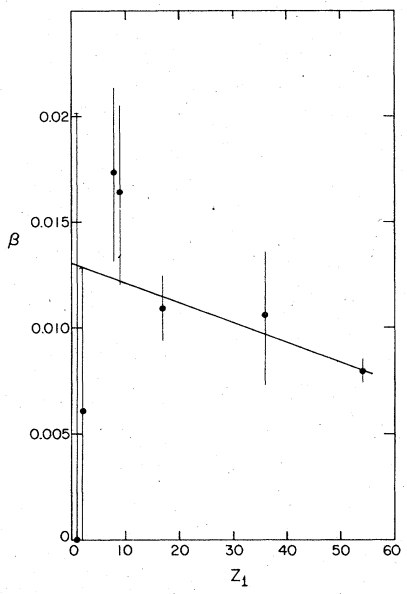

FIG. 6. Average final β value plotted against Z_1. Error bars represent standard deviation in the average.

approximately a ±25% scatter in the experimental cross sections, independent of Z_1 (except for Kr for which there is a 30%–40% scatter in the experimental cross sections). We attach little significance to the H and He values.

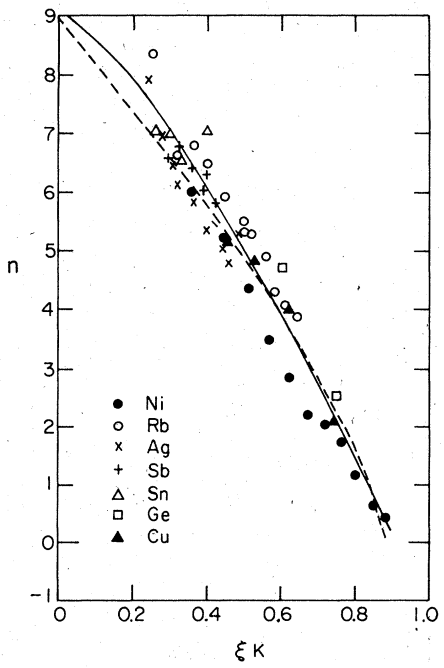

FIG. 7. Final n values plotted against ξ_K. Solid line gives least-squares polynomial fit to the data [Eq. (25)]. Dashed line shows final n values obtained in paper III [Eq. (16)].

For simplicity we assume that β should be a linear function of Z_1. The solid line in Fig. 6 is given by

$$\beta = 0.013 - 0.000\,092\,6 Z_1 . \tag{23}$$

The O and F β values are approximately 25% higher than the predictions of Eq. (23) suggesting that the experimental cross sections might be systematically high by 20%–30%. (The Cl cross sections might be 40%–50% low also.)

We investigated one other point. Using only Pb K-vacancy production cross sections in paper III, it was impossible to determine whether Z_F should be written as

$$Z_F = Z_2(1 + \beta Z_1) \tag{15}$$

or

$$Z_F = Z_2 + \delta Z_1 , \tag{24}$$

where δ is an adjustable function given by an equation similar to Eq. (23) and fitted in the same way as β. With R_{exp} values for many values of Z_2, we fitted our semiempirical formulas using both equations. We found no statistical evidence to conclude that Eqs. (1)–(5) and (8)–(15) predict the cross sections better than Eqs. (1)–(5), (8)–(14), and (24).

Figure 7 shows the final n values after iterating with Eqs. (1)–(5) and (8)–(15). The function shown by the solid line is given by

$$n(\xi_K) = 9.07 - 3.66\xi_K - 11.52\xi_K^2 + 5.25\xi_K^3 . \tag{25}$$

The dashed line in Fig. 7 gives the n values obtained in paper III [Eq. (16)]. The introduction of new Coulomb-deflection and relativistic correction factors in this paper clearly affects the n values, and hence, the binding correction factor, very little. This provides further justification for using the paper-III n values in comparing the atomic relativistic and Coulomb correction factors with theory [Figs. 3 and 4, Eqs. (18) and (20)]. Not only are the binding modifications small for proton and alpha-particle excitation, but the n values assumed in Secs. IV A–IV C are consistent with the final choice of the relativistic and Coulomb-deflection correction factors.

E. Predicted cross sections

To summarize, 1sσ-vacancy production cross sections can be predicted from the PWBA and Eq. (3) using Eqs. (4), (5), and (25) for the binding correction factor B, Eqs. (8) and (13) with $k = 0.25$ for the Coulomb factor C, and Eqs. (9)–(11), (14), (15), and (23) for the relativistic correction factor R. Figures 8–13 compare a large collection of measured K-vacancy production cross sections

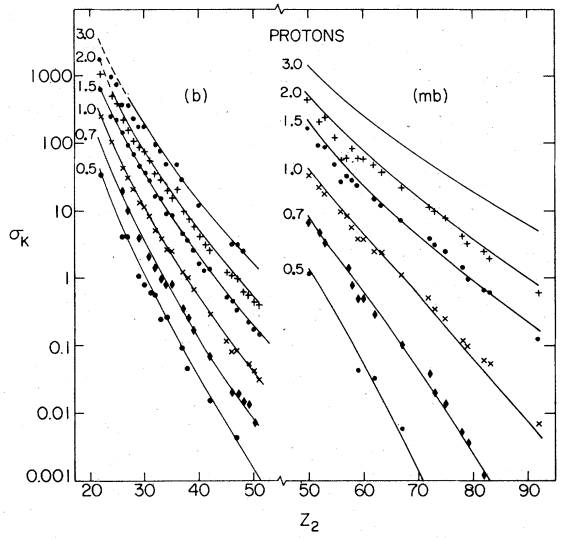

FIG. 8. Experimental proton-induced K-vacancy production cross sections in b and mb taken from Refs. 19, 22–35, and Table I (points) vs target atomic number. The lines give predictions of the semiempirical theory. (Cross sections predicted by the dashed part of the line have $\xi_K > 1$, where the binding correction factor is uncertain.) Numbers represent projectile bombarding energy in MeV/amu. Different symbols are used for different bombarding energies.

with these predictions. The proton and alpha-particle data is from our work and from Refs. 19 and 22–35. Because of the large number of measurements, in Figs. 8 and 9 we have not distinguished measurements taken by different groups; the symbols distinguish different projectile energies. Where overlapping measurements are available, a simple average is shown. Fewer measurements of O-, F-, and Cl-induced cross sections for $39 < Z_2 < 92$ have been made; however, we show a few thin-target cross sections from Refs. 30 and 36–38.

The agreement between experiment and our semiempirical theory is very good. There are

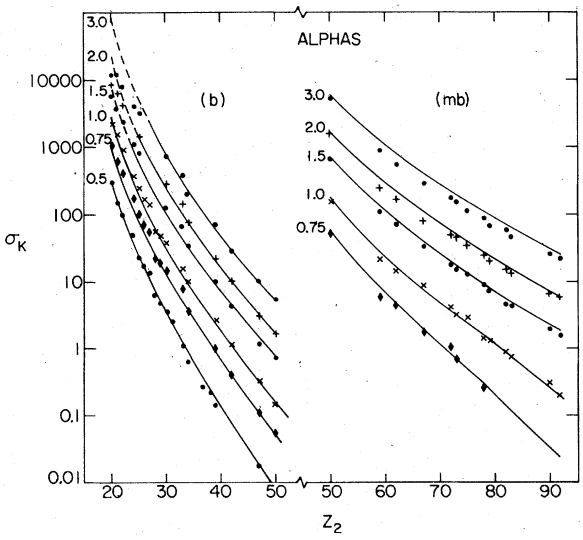

FIG. 9. Experimental alpha-particle-induced K-vacancy production cross sections. (See Fig. 8.)

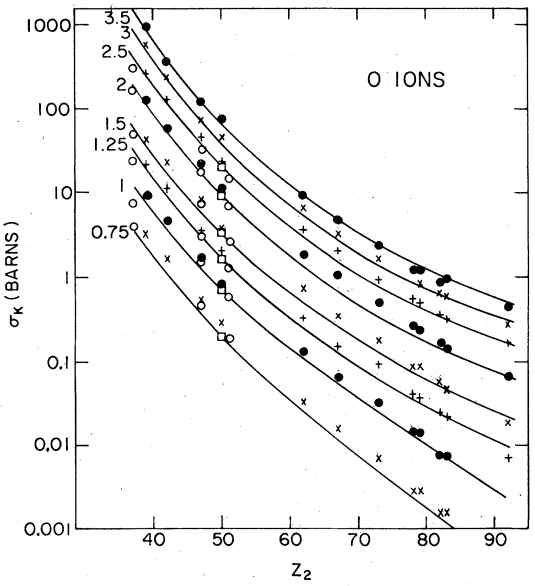

FIG. 10. K-vacancy production cross sections induced by 0.75- to 3.5-MeV/amu O ions plotted against target atomic number. (See Fig. 8.) Open circles from Ref. 37, open squares from Ref. 36.

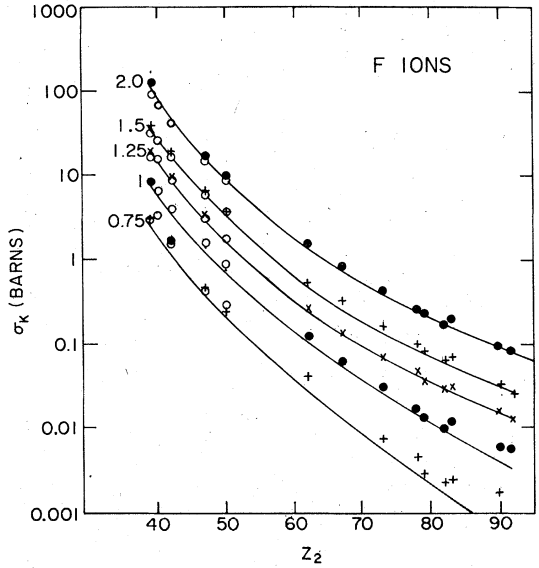

FIG. 11. K-vacancy production by 0.75- to 2-MeV/amu F ions. (See Fig. 8.) Open circles from Ref. 30.

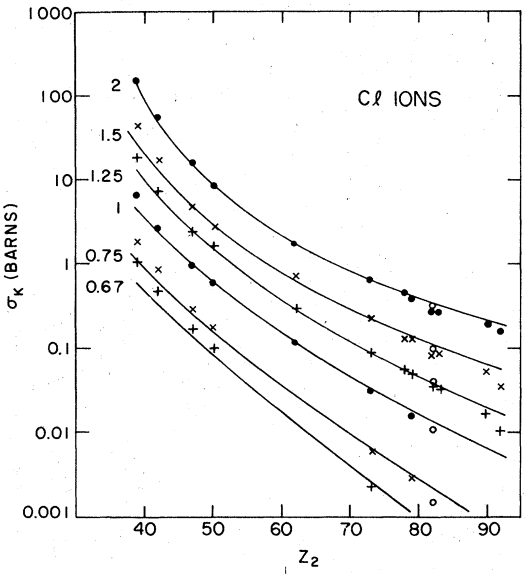

FIG. 12. K-vacancy production by 0.66- to 2-MeV/amu Cl ions. (See Fig. 8.) Open circles from Ref. 38.

some obvious discrepancies, many of which can be attributed to the data itself. For instance we see that the 2-MeV H^++ Te, I points disagree with the trend seen in the other measurements (and theory). Other examples can be observed. Also, the experimental alpha-particle cross sections seem to be consistently lower than theory in the high-Z elements for high bombarding energies. This is mostly our data. Further measurements of K-vacancy production in the heavy elements at higher bombarding energies should perhaps be made.

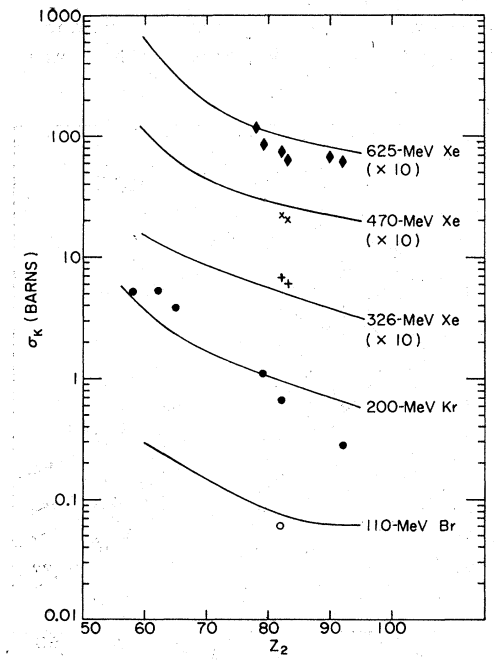

FIG. 13. K-vacancy production by Kr and Xe ions. (See Fig. 8.) Open circles from Ref. 38.

The 0.67–1.5 MeV/amu Cl + Y, MO, and Ag K-vacancy production sections are as much as 50% higher than theory. We noted in Sec. II that charge exchange effects[17] may be important in these collisions. When charge exchange effects are present, the use of the Merzbacher-Lewis formula to extract cross sections from thick-target yields is not valid. We thus conclude from the observed deviations in Fig. 12, and from estimated charge exchange influences,[10] that the experimental Cl + Y,..., Ag cross sections listed in Table I do not represent single-collision cross sections.

Plotted over seven decades the agreement between experiment (exp) and the semiempirical theory (se) may look better than it actually is. A better measure of the agreement is ratio σ_{exp}/σ_{se}. Table III summarizes the average ratio σ_{exp}/σ_{se} for a large number of H-, He-, O-, F-, Cl-, Kr(Br)-, and Xe-induced cross sections observed at fixed bombarding energies: 0.5, 0.67, 0.75, 1, 1.25, 1.5, 2, 2.5, 3, and 3.5 MeV/amu. Where different groups obtained different values for the same cross section, we took a simple average of the results. In many cases, to obtain cross sections at a given bombarding energy, an interpolation between closely spaced energies could be made. A few ratios greater than 1.5 or less than 0.5 were rejected. Table III shows that on the average experiment and the semiempirical theory agree within 15%. (The Kr-induced cross sections shown in Fig. 13 have a larger experimental uncertainty because measurements were made at a single bombarding energy only; hence the $dY_x dE_1$ values needed to convert yields to cross sections were just estimated.) It should be emphasized that experimental uncertainties are of the order

TABLE III. Average ratios of measured cross sections to the semiempirical predictions. (N is the number of measured cross sections.)

Z_1	N	σ_{exp}/σ_{se} [a]
H	290	0.88 ± 0.13
He	170	0.97 ± 0.14
O	94	1.11 ± 0.15
F	63	1.12 ± 0.11
Cl	61	1.01 ± 0.18
Kr(Br)	7	1.07 ± 0.49
Xe	11	0.90 ± 0.21

[a] Error represents standard deviation in the simple average.

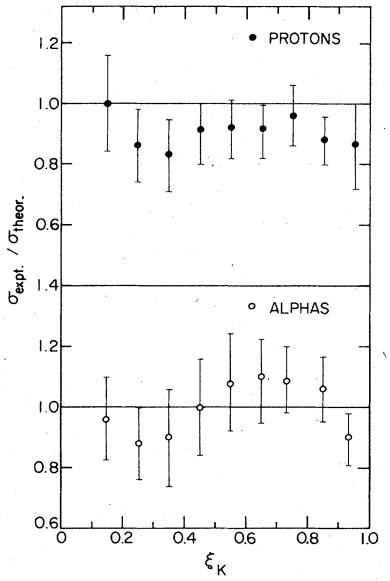

FIG. 14. The average ratio of the observed K-vacancy cross section to the semiempirical cross section vs ξ_K. Bars indicate standard deviation of the average.

of ±25% when the thick-target-yield method is used to measure K-vacancy cross sections, and, at best, ±10% when Rutherford monitoring is used.[19] Hence the semiempirical theory agrees with experiment to within somewhat better than the experimental error. More accurate measurements of $1s\sigma$-vacancy production cross sections are needed before the semiempirical formula can be further improved.

Finally we also show the averaged ratio σ_{exp}/σ_{se} for proton and alpha-particle excitation as a function of ξ_K in Fig. 14. From this study and similar studies for O, F, and Cl excitation we conclude that there is no definite ξ_K-dependent deviation between experiment and the semiempirical theory.

V. CONCLUSIONS

This work has verified the Kocbach Coulomb-deflection factor and the relativistic correction factor calculated by Anholt. A new semiempirical formula for calculating $1s\sigma$-vacancy production cross sections has been derived. Agreement between experiment and the semiempirical formula is within experimental error for collisions with projectiles with $Z_1 < 54$, reduced velocities $v_1/v_K \lesssim 0.5$ (or $\xi_K < 1$), and target atoms with $Z_2 > 20$ (or $Z_2 + Z_1 \gtrsim 25$). Within these restrictions we conclude that the $1s\sigma$-vacancy production cross sections are well understood.

ACKNOWLEDGMENTS

The author wishes to thank Jack Harris for considerable technical assistance in making the experiments with low-energy protons possible. Dave Clark and W. E. Meyerhof kindly assisted in the data taking. Discussions with W. E. Meyerhof, P. Amundsen, and L. Kocbach were very useful. This work was supported in part by the NSF.

*Present address: GSI, P. O. Box 541, 6100 Darmstadt 1, W. Germany.

[1]E. Merzbacher and H. W. Lewis, *Handbuch der Physik* (Springer-Verlag, Berlin, 1958), Vol. 34, p. 166.
[2]G. S. Khandelwal, B. H. Choi, and E. Merzbacher, At. Data 1, 103 (1969).
[3]D. Jamnik and C. Zupancic, Kl. Dan. Vidensk. Selsk. Mat.-Fys. Medd. 31, No. 2 (1957).
[4]J. Bang and J. M. Hansteen, Kl. Dan. Vidensk. Selsk. Mat.-Fys. Medd. 31, No. 13 (1959).
[5]J. M. Hansteen, O. M. Johnsen, and L. Kocbach, At. Data Nucl. Data Tables 15, 305 (1975).
[6]P. A. Amundsen, L. Kocbach, and J. M. Hansteen, J. Phys. B 9, L203 (1976).
[7]P. A. Amundsen, J. Phys. B 9, 971 (1976).
[8]L. Kocbach, Phys. Norv. 8, 187 (1976).
[9]W. Brandt, R. Laubert, and I. Sellin, Phys. Lett. 21, 518 (1966); G. Basbas, W. Brandt, and R. Laubert, Phys. Rev. A 7, 983 (1973).
[10]R. Anholt and W. E. Meyerhof, Phys. Rev. A 16, 190 (1977).
[11]W. Lichten, Phys. Rev. 164, 131 (1967); M. Barat and W. Lichten, Phys. Rev. A 6, 211 (1972).
[12]W. E. Meyerhof, R. Anholt, T. K. Saylor, S. M. Lazarus, A. Little, and L. F. Chase, Jr., Phys. Rev. A 14, 1953 (1976).
[13]R. Anholt, Phys. Rev. A 17, 976 (1978), preceding paper.
[14]D. Ward, J. S. Forster, H. R. Andrews, I. V. Mitchell, G. C. Ball, W. G. Davies, and G. J. Costa, Compilation of Realistic Stopping Powers for ^{4}He Ions, Chalk River Report No. AECL-4914 (1975).
[15]J. S. Forster, D. Ward, H. R. Andrews, G. C. Ball, G. Costa, W. G. Davies, and I. V. Mitchell, Nucl. Instrum. Methods 136, 349 (1976).
[16]W. Brandt and R. Laubert, Phys. Rev. A 11, 1233 (1975).
[17]T. J. Gray, P. Richard, K. A. Jamison, and J. M. Hall, Phys. Rev. A 14, 1333 (1976).
[18]W. Bambynek, E. Crasemann, R. W. Fink, H. U. Freund, H. Mark, C. D. Swift, R. E. Price, and V. P. Rao, Rev. Mod. Phys. 44, 716 (1972).
[19]T. L. Criswell and T. J. Gray, Phys. Rev. A 10, 1145 (1974).
[20]R. S. Hager and E. C. Seltzer, Nucl. Data A 4, 1 (1968).
[21]I. Y. Lee (private communication); see, for example, T. Inamura, F. Kearns, G. Varley, and J. C. Lisle, Nucl. Phys. A 270, 255 (1976).
[22]R. C. Bearse, D. A. Close, J. J. Malanify, and C. J.

Umbarger, Phys. Rev. A 7, 1269 (1973).
[23]G. A. Bissinger, S. M. Shafroth, and A. W. Waltner, Phys. Rev. A 5, 2046 (1972).
[24]J. L. Duggan, R. P. Chaturvedi, C. C. Sachtleben, and J. Lin, private communication as quoted in Ref. 34.
[25]D. V. Ferree, Ph.D. thesis (University of Tennessee, 1972).
[26]N. Khelil and T. J. Gray, Phys. Rev. A 11, 893 (1975).
[27]R. D. Lear and T. J. Gray, Phys. Rev. A 8, 2469 (1973).
[28]L. M. Winters, J. R. MacDonald, M. D. Brown, L. D. Ellsworth, and T. Chiao, Phys. Rev. A 7, 1276 (1973).
[29]S. R. Wilson, F. D. McDaniel, J. R. Rowe, and J. L. Duggan, Phys. Rev. A 16, 903 (1977).
[30]F. D. McDaniel (private communication).
[31]R. F. Carlton, J. L. Duggan, J. Lin, K. Eger, M. T. Lu, M. J. Kelley, J. R. Dunning, and H. D. Fetzer, Bull. Am. Phys. Soc. 17, 89 (1972).
[32]F. D. McDaniel, T. J. Gray, and R. K. Gardner, Phys. Rev. A 11, 1607 (1975).
[33]J. Lin, J. L. Duggan, and R. F. Carlton, Proceedings of the International Conference on Inner-Shell Ionization Phenomena, 1973, Conf. 720404 (U.S. AEC), Vol. 2, p. 988.
[34]T. J. Gray, Tables for K-Shell X-ray Analysis by Protons and ^{4}He Ions (private communication, 1975).
[35]C. H. Rutledge and R. L. Watson, At. Nucl. Data 12, 195 (1973).
[36]C. C. Sachtleben, J. L. Duggan, and R. P. Chaturvedi, Bull. Am. Phys. Soc. 18, 103 (1973).
[37]T. J. Gray, P. Richard, R. L. Kaufmann, T. C. Holloway, R. K. Gardner, G. M. Light, and J. Guertin, Phys. Rev. A 13, 1344 (1976).
[38]D. Burch, W. B. Ingalls, H. Wiemann, and R. Vandenbosch, Phys. Rev. A 10, 1254 (1974); D. Burch (private communication).